Natural Convection and Radiation in Enclosures with Semi-transparent Medium: Conjugate CFD Analysis

E. G. Barbosa[1†], M. E. V. Araujo[1], M. A. Martins[1] and E. G. Barbosa[2]

[1] *Federal University of Viçosa, Department of Engineering, Viçosa, Minas Gerais, 36570-900, Brazil*
[2] *Federal University of São Carlos, Department of Chemistry, São Carlos, São Paulo, 13565-905, Brazil*

†*Corresponding Author Email: eloinyguimaraes@outlook.com*

ABSTRACT

Radiation heat transfer is often ignored in several studies as it has few significant effects in some cases. However, when using a participating fluid, where the molecules interact with the radiative spectrum, these effects cannot be disregarded. A numerical study of the heat transfer by natural convection and radiation in two square enclosures (with and without protrusions) using a transparent (non-participating) and semi-transparent (participating) fluid medium was carried out in this study. The governing equations were discretized using the finite volume technique and solved using a CFD code ANSYS CFX. The heat transfer by radiation was modeled using the differential approach. The model proposed in this study was validated with the data available in the literature with errors of less than 3%. The results showed that the addition of the participant fluid (CO_2) promotes a better condition for heat transfer. It was proven that the use of the participating medium caused an increase in the Nusselt number, indicating an increase in heat transfer by convection. The presence of protrusions reduces the thermal stratification zone for the pure convection case (CP) and provides a better temperature distribution for the cases conjugated with air (CR_{AIR}) and CO_2 (CR_{CO2}) when compared to the cases without protrusions. It is observed that for all cases, the geometry with protrusion presented the highest values for the Nusselt number, indicating that the insertion of the protrusion increases the heat transfer in the enclosure by up to 11%. The airflow values for the conjugated cases are more than 300% higher than those presented for the pure convection case for any Rayleigh number value. The heat flow increased by up to 4 times when the radiation effect was considered. The average Nusselt number increased with the increase in the Rayleigh number and with the coupling of radiation in the energy equation. This indicates that the effect of radiation cannot be disregarded in the study of heat transfer in enclosures.

Keywords: Coupled heat transfer; Heat flow; Nusselt number; Participating fluid; Rayleigh number.

NOMENCLATURE

a	linear anisotropy coefficient	Nu	Nusselt number
CP	Pure convection case	p	pressure
CR_{AIR}	conjugated convection-radiation case using air	Pr	Prandtl number
CR_{CO2}	conjugated convection-radiation case using CO_2	q''	average heat flux
c_p	specific heat	q_{rad}	fraction of radiant thermal energy
$E_{b\lambda}$	energy spectrum for radiation emitted by a blackbody	Ra	Rayleigh number
		T	temperature
g	gravitational acceleration	T_H	hot wall temperature
G_λ	spectral incident radiation	T_C	cold wall temperature
h	heat transfer coefficient	u, v	horizontal and vertical velocity components
H_P	height of the protrusion		
$I_{\lambda bw}$	black body intensity	x, y	horizontal and vertical coordinates
k	thermal conductivity of the fluid	β	coefficient of volumetric expansion
$K_{a\lambda}$	absorption coefficient	$\varepsilon_{\lambda w}$	emissivity
$K_{s\lambda}$	scattering coefficient	μ	dynamic viscosity
L_P	width of the protrusion	ρ	density of fluid
L	enclosure's dimension	ΔT	temperature difference

1. INTRODUCTION

Heat transfer by convection and radiation has been the focus of numerous studies carried out over the years (Wang *et al.* 2014, Meng *et al.* 2016, Pishkar *et al.* 2022). The significant interest in such problems is due to their importance in a wide range of engineering applications, such as the thermal design of buildings (Li and Tu 2019), radiation cooling systems (Cui *et al.* 2016), cooling of electronic components (Oguntala *et al.* 2019), thermal processing of mobile plates (Saedodin and Barforoush 2014), heat exchangsers (Gireesha *et al.* 2020), solar collectors (Karimipour 2017), nuclear reactors (Tsuji *et al.* 2014), among others.

The effect of thermal radiation on the temperature and flow fields has been neglected in studies on enclosures (Rashidi *et al.* 2014, Saha and Gu 2015), aiming to simplify the analysis of heat transfer, under the justification of expected low temperatures. However, it has been shown that radiation can have a significant influence on such problems, even at low temperature levels (Dehbi *et al.* 2019). It is known that the natural convection in the enclosure is strongly influenced by the temperature difference and the action of the gravitational force (Patil *et al.* 2016). Besides, radiation can modify the temperature distribution of the wall and the flow patterns that, in turn, affect the natural convection, producing interaction effects (Sharma *et al.* 2007).

In recent years, several numerical and experimental studies have been carried out to investigate the effects of natural convection coupled with radiation in enclosures. A numerical analysis of the complex heat transfer (natural convection, conduction, and radiation) in a rectangular enclosure with a heat source was performed by Miroshnichenko *et al.* (2016). The study proved that the convective Nusselt number is an increasing function of the Rayleigh number and a decreasing function of the surface emissivity. Patil *et al.* (2016) numerically studied the combined heat transfer of natural convection and radiation in a square cabinet with protrusions. The authors found that the allocation of protrusions in the corners of the cabinet considerably increases the number of Nusselt. Saravanan and Raja (2020) evaluated the effect of heater arrangements on thermal radiation combined with natural convection in a square enclosure. It was observed that when the heaters were placed side by side, radiation plays a fundamental role in changing the flow pattern, while the reverse was observed when the heaters were placed one above the other. It is known that the influence of thermal radiation on the general heat transfer of enclosures is more significant depending on the type of fluid by which the medium is filled, such as transparent, semitransparent, and participating fluids (Dehbi *et al.* 2019).

According to the substance of the medium and its thickness, two different approaches can be used to describe the effect of radiation on heat transfer in enclosures. A transparent medium allows an electromagnetic wave to pass through it without any attenuation, this definition is generally used for pure gases such as air. Thus, surface radiation must be coupled with natural convection only at the enclosure flow limits (Modest 2013). Most studies of natural convection coupled with surface thermal radiation fall within this approach (Sharma *et al.* 2007, Ibrahim *et al.* 2013, Ahmed *et al.* 2014, Saravanan and Raja 2020, Mikhailenko *et al.* 2021). On the other hand, a semi-transparent medium causes partial attenuation when in contact with an electromagnetic wave. Thus, in addition to the radiation effects at the boundaries, a radiant transport equation must be solved to simulate the scattering and absorption effects along the radiation beams (Modest 2013). Contrary to what was observed for transparent media, this type of approach still represents the smallest part of studies on the topic (Meftah *et al.* 2009, Goodarzi *et al.* 2014, Karimipour 2017).

As demonstrated in the literature review, although the evaluation of the effect of radiation and natural convection conjugated in semi-transparent media has been performed for some cases, this problem has not yet been very well documented. It is precisely in this context that this work fits. This is one of the few reports in the literature that evaluates the effect of the use of participating media on the conjugated heat transfer in enclosures. In this study, the geometry considered is a square enclosure with two opposite vertical walls differentially heated and two insulated walls. Three different approaches to heat transfer are evaluated, compared, and discussed in detail. The first considers only the case of pure convection in the enclosure, the second considers convection conjugated with radiation for a transparent fluid, and the last considers convection conjugated with radiation for a semi-transparent fluid. In the first and second evaluations, the air is used as a transparent medium, so that radiative heat transfer occurs only between the enclosure walls. As for the last evaluation, CO_2 was used as a semi-transparent fluid, also participating in heat transfer by radiation. In addition, an evaluation of the use of protrusions in enclosures of different sizes was also carried out, to verify the effects of these parameters on the conjugate heat transfer.

2. PHYSICAL AND MATHEMATICAL MODEL

2.1 Geometric Description

In this study, a two-dimensional square enclosure with dimension L was considered. Two polygonal protrusions were positioned at the upper and lower ends of the enclosure. The dimensions of both protrusions are width (L_P) of 0.2 L and height (H_P) of 0.23 L. The physical model is shown in Fig. 1. The enclosure used in this study contains adiabatic walls in the horizontal direction and isothermal walls at different temperatures in the vertical direction. The temperature difference (ΔT) between the hot wall (T_H) and the cold wall (T_C) was 10 °C, for all cases evaluated. Two types of fluids were investigated as a means of filling the enclosure, being a transparent, non-participating fluid (air) and a semitransparent and participating fluid (CO_2). The gravity vector was considered to be acting parallel to the y-axis. The

investigations were carried out for different Rayleigh numbers (10^4, 10^5 e 10^6) and to the enclosure with and without the presence of protrusion. Three different cases of heat transfer are evaluated: CP - pure convection, CR_{AIR} - convection conjugated with radiation for a transparent medium, and CR_{CO2} - convection conjugated with radiation for a semi-transparent medium. In the first and second evaluations, the air is used as a transparent medium, while for the last evaluation, CO_2 is used as a semi-transparent fluid.
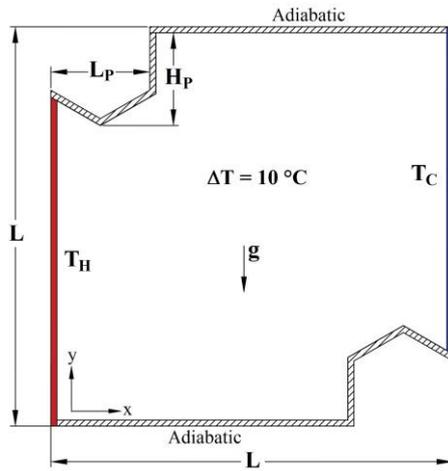
Fig. 1. Physical model of the enclosure considered in this study.

2.2 Governing Equations and Radiation Model

For all cases evaluated in this study, the number of Rayleigh investigated ranged from 10^4 to 10^6. For the considered conditions, the number of Prandtl was 0.71 and 0.75 for air and CO_2, respectively. Air and CO2 were modeled as gases with constant properties, with variation only for density. The flow was considered to be incompressible and the viscous heat dissipation and compressibility effects are negligible. Buoyancy was modeled using Boussinesq's approximation. The wall thickness is thin and therefore the conduction of heat can be neglected. The surfaces of the walls were assumed to be gray, opaque, and diffuse. Investigations were carried out on steady-state. Based on these premises, the following equations were used, conservation of mass (Eq. 1), conservation of the amount of movement in X (Eq. 2) and Y (Eq. 3), and the conservation of energy (Eq. 4). Where, "u" and "v", represent the horizontal and vertical velocity components, respectively, ρ the density, μ the dynamic viscosity, "p" the pressure, "g" the gravitational acceleration, β coefficient of volumetric expansion, "T" the temperature, c_p the specific heat, and κ the thermal conductivity.

The mechanisms used to describe the heat transfer in the enclosure were radiation and laminar natural convection. For CR_{AIR} and CR_{CO2} cases, the effects of the interaction between thermal radiation and natural convection in the enclosure were analyzed. A radiation heat generation term (q_{rad}) was added to the

fluid energy equation to model the radiant thermal energy in the enclosure. Equation 5 was used to model radiative transfer (RTE) in the participating medium (Modest 2013). Where "a" represents the absorption coefficient, "n" the refractive index, "r" position, "s" direction, "I" the radiative intensity, Φ the phase function, Ω the solid angle, and σ_s is the scattering coefficient equal to zero (Siegel *et al.* 2010, Nia *et al.* 2018).

Because of the high computing costs associated with the solution of the radiative transfer equation (RTE), affordable implementations resulting in a substantial simplification have been devised (Eby *et al.* 1998, Modest 2013). In this study, the P1 model has been investigated. The first-order spherical harmonic approximation (P1 model) was used for the RTE equation. In this model, a series based on spherical harmonics can be used to express the radiation intensity, and the P1 equation is obtained by truncating orders greater than 2 according to Eq. 6. Or in general form in Eqs. 7 and 8. Where G_λ represents the incident radiation. For a detailed derivation of these equations, the reader is directed to Modest (2013).

Equation 9 is obtained by combining Eqs. 7 and 8, forming a second-order partial differential equation. Substituting the $q_{rad\lambda}$ term in the RTE equations it is possible to obtain Eq. 10 which represents a general form for spectral incident radiation (Araujo *et al.*, 2022). Applying this equation to the boundary conditions of the enclosure, we obtain Eq 11. Where λ_w represents the spectral emissivity of the wall, $\overrightarrow{n_w}$ normal vector and $I_{\lambda bw}$ the blackbody intensity (Goebel and Mundt, 2011). In this work, the walls were considered as gray surfaces with emissivity ($\varepsilon_{\lambda w}$) equal to 0.85.

The heat transfer through the enclosure was characterized by the Nusselt mean number (N_{um}) which was calculated according to Eq. 12 (Meftah *et al.* 2009, Moufekkir *et al.* 2012a). T_H and T_C represent the hot and cold wall temperatures, respectively, and "L" represents the characteristic length of the enclosure.

$$\frac{\partial u}{\partial x} + \frac{\partial v}{\partial y} = 0 \qquad (1)$$

$$\rho \left(u \frac{\partial u}{\partial x} + v \frac{\partial u}{\partial y} \right)$$
$$= -\frac{\partial p}{\partial x} \qquad (2)$$
$$+ \mu \left[\frac{\partial^2 u}{\partial x^2} + \frac{\partial^2 u}{\partial y^2} \right]$$

$$\rho \left(u \frac{\partial v}{\partial x} + v \frac{\partial v}{\partial y} \right) \qquad (3)$$
$$= -\frac{\partial p}{\partial y}$$
$$+ \mu \left[\frac{\partial^2 v}{\partial x^2} + \frac{\partial^2 v}{\partial y^2} \right]$$
$$+ g \beta (T - T_0)$$

$$\rho c_P \left(u \frac{\partial T}{\partial x} + v \frac{\partial T}{\partial y} \right)$$
$$= \kappa \left[\frac{\partial^2 T}{\partial x^2} + \frac{\partial^2 T}{\partial y^2} \right] \tag{4}$$

$$\frac{dI(r,s)}{ds} + (a + \sigma_s)I(r,s)$$
$$= an^2 \frac{\sigma T^4}{\pi} + \frac{\sigma_s}{4\pi} \int_0^{4\pi} I(r,\acute{s}) \, \Phi(s,\acute{s}) d\acute{\Omega} \tag{5}$$

$$q_{rad,\lambda} = -\frac{1}{3a_\lambda} \nabla G_\lambda \tag{6}$$

$$q_{rad,\lambda} = -\frac{1}{3(K_{a\lambda} - K_{s\lambda}) - A \, K_{s\lambda}} \nabla G_\lambda \tag{7}$$

$$\nabla q_{rad,\lambda} = a_\lambda (4\pi I_{\lambda b} - G_\lambda) \tag{8}$$

$$\nabla \cdot \left(\frac{1}{3a_\lambda} \nabla G_\lambda \right) = a_\lambda (G_\lambda - 4\pi I_{\lambda b}) \tag{9}$$

$$\nabla \cdot \left(\frac{1}{3(K_{a\lambda} - K_{s\lambda}) - A \, K_{s\lambda}} \nabla G_\lambda \right)$$
$$= K_{a\lambda}(G_\lambda - 4E_{b\lambda}) \tag{10}$$

$$G_\lambda - \frac{2}{3a_\lambda} \left(\frac{2 - \varepsilon_{\lambda w}}{\varepsilon_{\lambda w}} \right) \nabla G_\lambda \cdot \overrightarrow{n_w}$$
$$= 4\pi I_{\lambda b} w \tag{11}$$

$$Nu_m$$
$$= \frac{1}{(T_H - T_C)} \int_0^L \left| \frac{\partial T}{\partial x} \right|_{x=0 \; or \; L} dy$$
$$+ \frac{1}{\kappa(T_H - T_C)} \int_0^L q_{rad}|_{x=0 \; or \; L} \, dy \tag{12}$$

2.3. Numerical Method and Boundary Conditions

The governing equations were discretized by the control volume-based discretization method and solved in Ansys CFX v19.2. The second-order upwind approximation scheme was employed for the conservation of energy and momentum. Diffusive terms were approximated by central differences. SIMPLE algorithm has been used to resolve the pressure–velocity coupling. The first-order spherical harmonic approximation (P1 model) was used to couple the effects of radiation acting on the fluid. The Monte Carlo method was used to model the radiation on the walls of the enclosure and its effect on the participating fluid. A mean square error (RMS) below 10^{-4} was used as a convergence criterion for the continuity, energy, and momentum equations. The maximum number of iterations adopted in the simulation was 1000.

The boundary conditions used in this study are: non-slip condition on solid walls, that is, u = v = 0; The enclosure was considered differentially heated. The left side wall is isothermal, where x = 0 and T = T_H; The right side wall is isothermal, where x = L and T = T_C; The upper (y = L) and lower (y = 0) walls of the enclosure are considered adiabatic; The heat transfer on the right and left surfaces of each part of the enclosure is the same; About working fluids: the air was considered perfectly transparent, and therefore, only solid surfaces contribute to the exchange of heat for radiation; CO_2 was considered semi-transparent and participant, and therefore, the fluid also contributes to the exchange of heat for radiation.

2.4. Details and Mesh Independence Test

The meshes used in this study were generated in the commercial meshing tool ANSYS ICEM-CFD. The meshes are composed of hexahedral elements, and to accurately capture temperature and velocity gradients near the walls, a finer mesh resolution was applied at these boundaries, with thicker cells extending towards the enclosure core. This mesh distribution and the local refinement close to the walls were applied in all cases evaluated. Figure 2 shows in detail the computational mesh distribution for the physical domain of L = 0.025m for the case of the enclosure with protrusion.

The results of the mesh independence tests for all evaluated cases are shown in Table 1. The meshes used are highlighted in bold in the table.

To ensure the independence of the results regarding errors associated with special and temporal discretization, an evaluation of different mesh sizes was performed. Successive mesh refinements were performed until the Nusselt number variation was
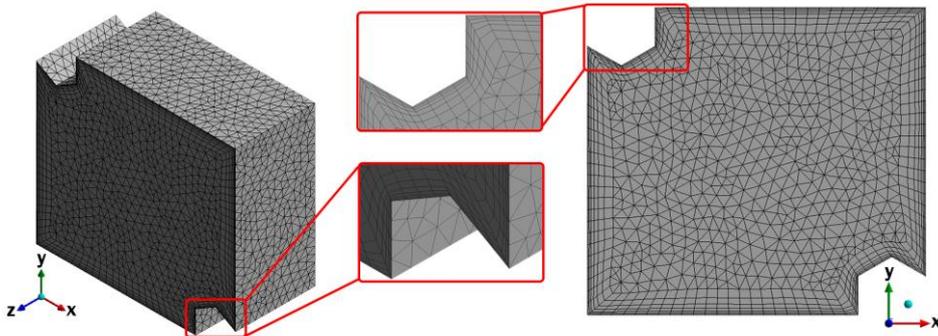
Fig. 2. Details and distribution of the computational mesh for the physical domain of L = 0.025m for the case with protrusion.

Table 1 Mesh independence test for cases with and without protrusion and Rayleigh numbers ranging from 10^4 to 10^6

Cases without Protrusion					
Rayleigh Number	Nodes	Elements	Nusselt CP	Nusselt CR_{Air}	Nusselt CR_{CO2}
Ra 10^4	3,007	7,011	2.226	7.722	13.593
	7,209	20,413	2.232	7.737	13.613
	16,289	**51,052**	**2.236**	**7.749**	**13.630**
	25,526	84,968	2.238	7.754	13.639
Ra 10^5	6,951	20,114	4.610	16.851	29.835
	19,087	64,379	4.618	16.879	29.873
	45,953	**172,961**	**4.625**	**16.900**	**29.910**
	76,096	303,948	4.629	16.911	29.919
Ra 10^6	23,885	86,267	9.060	36.245	64.145
	64,491	262,436	9.075	36.302	64.252
	112,932	**488,702**	**9.086**	**36.340**	**64.330**
	116,016	501,672	9.093	36.350	64.352
Cases with Protrusion					
Rayleigh Number	Nodes	Elements	Nusselt CP	Nusselt CR_{Air}	Nusselt CR_{CO2}
Ra 10^4	2,611	6,045	2.520	8.565	15.120
	6,590	18,007	2.524	8.579	15.139
	15,046	**46,401**	**2.528**	**8.591**	**15.158**
	24,939	84,109	2.530	8.598	15.168
Ra 10^5	6,745	19,436	5.188	18.875	33.122
	18,332	62,525	5.195	18.899	33.161
	43,583	**163,775**	**5.202**	**18.920**	**33.198**
	72,943	291,679	5.206	18.932	33.209
Ra 10^6	22,985	82,737	10.031	40.464	71.055
	65,055	267,187	10.045	40.512	71.146
	113,489	**498,125**	**10.058**	**40.557**	**71.227**
	123,014	510,922	10.064	40.574	71.289

less than 0.1% (Valh Davis, 1983). For both with protrusion and without protrusion cases, for Ra = 10^4 and Ra = 10^5 an overall element size of 0.9 mm was used, while for Ra = 10^6 this value was 1.0 mm. For all cases evaluated, a min size factor of 0.01 and a defeature size factor of 0.005 were applied. For local refinement near the walls, a transition rate of 0.77 and a growth rate of 1.2 were used.

3. DATA VALIDATION

The numerical model considered in this study was validated from the data obtained in the literature for square enclosures, with the working fluid being the air for the Rayleigh number range evaluated. Validation was performed for the scenario where only pure natural convection is considered, and also for the scenario of combined convection and radiation.

3.1. Pure Convection

The average Nusselt numbers on the hot wall of the enclosure as a function of the number of Rayleigh obtained in this study, compared to different values found in the literature can be seen in Table 2. The results presented by Vahl Davis (1983) and Baïri (2008) were obtained from experimental data, while those obtained by Bilgen and Oztop (2005), Vivek *et*

Table 2 Comparison of the average Nusselt number on the hot wall for different Rayleigh numbers with the reference data

Rayleigh number	Average Nusselt number on the hot wall of the enclosure				
	This study	Vahl Davis (1983)	Bilgen and Oztop (2005)	Vivek *et al.* (2012)	Patil *et al.* (2016)
10^4	2.236	2.243	2.245	2.246	2.230
10^5	4.544	4.519	4.521	4.527	4.410
10^6	8.832	8.800	8.800	8.801	8.630

Rayleigh number	This study	Baïri (2008)
26,454	3.169	3.200
485,476	6.431	6.491
76,654,326	26.617	26.820

al. (2012), and Patil *et al.* (2016) were obtained numerically. Observa-se que os dados apresentados para este estudo, estão de acordo com os obtidos experimentalmente, com erros inferiores a 1%, e também são próximos aos obtidos numericamente, com erros inferiores a 3%, which validates the pure convection model.

3.2. Conjugated Heat Transfer (Convection and Radiation)

The conjugated heat transfer scenario was validated based on the experimental data achieved by Bajorek and Lloyd (1982) and the numerical data by Patil *et al.* (2016). The dimensionless temperature profile at an average height (y / L = 0.5) was used, for a Rayleigh number of 10^5, a temperature difference of 15.5 °C, and a Prandtl number of 0.71. The validation is shown in Fig. 3. It can be seen that the temperature profile obtained in this study follows the expected behavior agreeing with those presented by the references and in this way, it can be considered that the conjugated heat transfer model was validated.
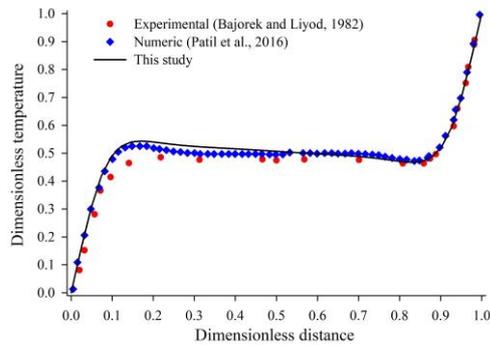
Fig. 3. Comparison of the dimensionless temperature profile along with the average height (y / H = 0.5) in the enclosure with the reference data.

4. RESULTS AND DISCUSSION

4.1. Flow patterns (current lines)

Figure 4 shows the current lines for the cases of pure convection (CP) and conjugated convection and radiation with air (CR_{AIR}) and CO_2 (CR_{CO2}), depending on the number of Rayleigh (Ra) for the enclosure without protrusions. A similar flow pattern was found for CP and CR_{AIR} cases in Ra 10^4 with a rotating cell in the enclosure core. This behavior is generally verified in typically laminar flows. For these cases, a greater area of stagnation was also observed near the enclosure walls, when compared to other cases. As the Ra increased, it was found that the flow becomes more intense at the edges of the enclosure and that the convective cell showed a diagonal movement in cases where radiation is considered (CR_{AIR} and CR_{CO2}). It can also be observed that with the increase in Ra, a large amount of fluid was restricted in the enclosure's core, presenting low-speed values.

Regarding the flow magnitude, it was found that the scenario in which convection and radiation are coupled and the working fluid is a participant (CR_{CO2}) presented the highest velocity values, followed by the CR_{AIR} case, for all evaluated Ra. The lowest speed values were observed for the CP case for the Ra range considered in this study. It was found that the highest velocity values were found close to the enclosure walls for both scenarios. It was also observed that an increase in the number of Ra caused an increase in speed values in all cases considered. When the Ra increased from 10^4 to 10^6, there were increases of 129, 115, and 90% in the maximum speed values for the cases of CP, CR_{AIR}, and CR_{CO2}, respectively. The highest observed velocity values were 0.030 m s^{-1} for Ra 10^4, 0.042 m s^{-1} for Ra 10^5, and 0.057 m s^{-1} for Ra de 10^6, both for the case of CR_{CO2}.
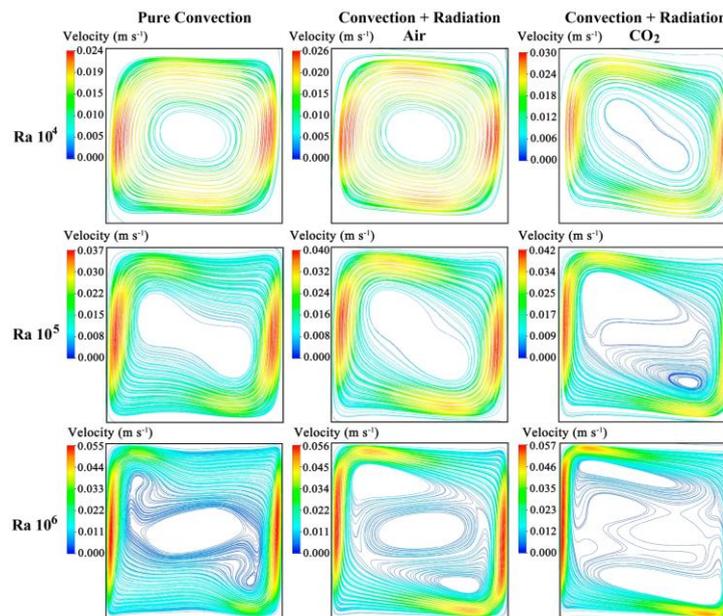
Fig. 4. Current lines of the evaluated cases CP (left), CR_{AIR} (middle) CR_{CO2} (right) as a function of the number of Ra for the enclosure without protrusions.
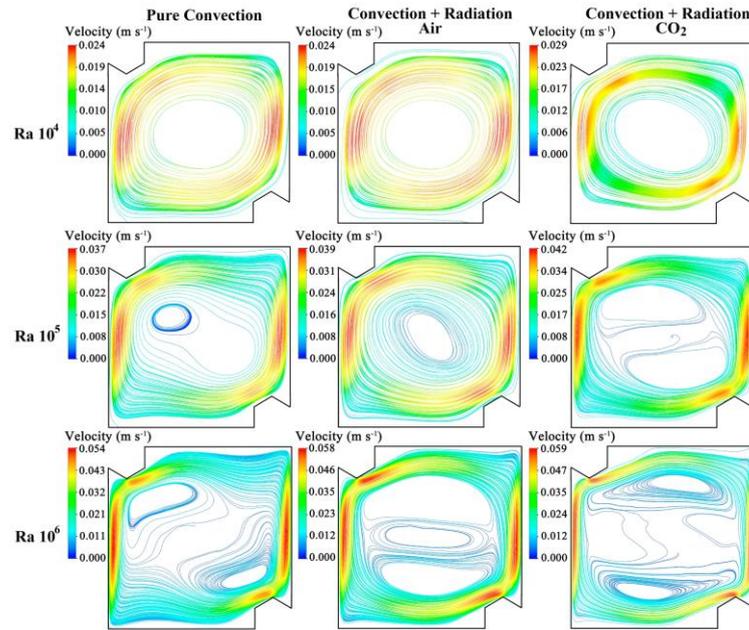
Fig. 5. Current lines of the evaluated cases CP (left), CR$_{AIR}$ (middle) CR$_{CO2}$ (right) as a function of the number of Ra for the enclosure with protrusions.
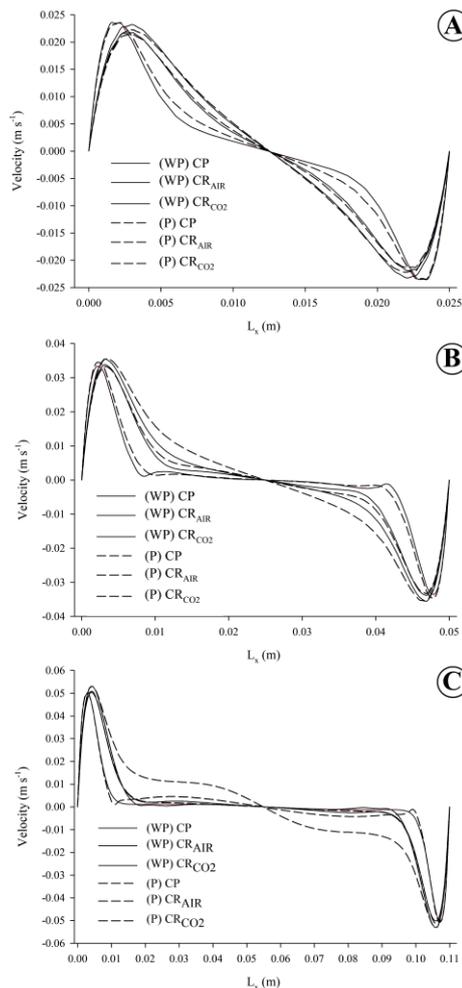
Fig 6. Velocity profiles along the enclosure in the x-axis direction for (A) L = 0.025m (Ra = 10^4); (B) L = 0.050m (Ra = 10^5) and (C) L = 0.110 m (Ra = 10^6).

Figure 5 shows the current lines for the cases of CP, CR$_{AIR}$, and CR$_{CO2}$ as a function of Ra, for the enclosure with protrusions. A behavior similar to that observed for the enclosure without protrusions was verified. The cases of CP and CR$_{AIR}$ for Ra 10^4 show the formation of a circular vortex in the center of the enclosure, characterized by the laminar regime. As the Rayleigh number increases, the flow intensifies in the regions near the walls and a large amount of the fluid is restricted in its core. However, zones of stagnation were found in the regions immediately to the right and left of the protrusions for all evaluated scenarios. Such zones reduce with the increase of Ra and the formation of secondary rotation cells from Ra of 10^5 occurs. The highest velocity values were found near the enclosure walls and near the protrusions. The presence of protrusions makes most of the current lines present higher speeds when compared to the enclosure without protrusions. This indicates a more intense flow. This fact was also observed by Patil *et al.* (2016) in their study of a rectangular enclosure with different protrusions.

Similar to what occurred for the enclosure without protrusions, an increase in the number of Ra caused an increase in speed values in all cases considered. The highest observed velocity values were 0.029 m s^{-1} for Ra 10^4, 0.042 m s^{-1} for Ra 10^5, and 0.059 m s^{-1} for Ra 10^6, both for the case of CR$_{CO2}$. These maximum speed values were close to those observed for the enclosure without protrusions. The case with the highest velocity values was CR$_{CO2}$ for all evaluated Ra.

For better visualization of the velocity profiles, horizontal lines were drawn in the center of the enclosures for all cases evaluated, and the velocity data along these lines can be seen in Fig. 6. Note that the increase in the size of the enclosures directly influences the maximum velocity reached. Despite

the temperature of the hot wall and the temperature gradient between the walls being the same for all cases, the cases of L = 0.110 m (Fig. 6c) presented the highest velocities, being up to 125% higher compared to the case of L = 0.025m. The maximum speeds reached for the cases of L = 0.025, 0.050 and 0.110 m were 0.0235; 0.0355 and 0.0530 m s^{-1}, respectively. However, the mean velocity along the central line was similar for all cases, being this in the magnitude of 0.01 m s^{-1}. This may be related to the higher Rayleigh number observed for these cases, consequently indicating a greater effect of buoyancy forces in relation to viscous ones. Evaluating Figs. 4, 5, and 6, it is noted that a great acceleration is reached after a certain distance from the heated wall of the enclosures, in all cases evaluated. This is because a greater heat transfer occurs close to the walls, which leads to an intensification of the fluid movement close to these surfaces. Similar behavior was also observed by Abu-Nada and Oztop (2009) when evaluating the effect of tilt angles on natural convection in enclosures filled with nanofluid.

4.2. Temperature Profile (Isotherms)

Figure 7 shows the temperature distribution of the enclosure without protrusions for the cases evaluated in this study and the Ra ranging from 10^4 to 10^6. The effect of isotherms tending to remain in an upright position indicates that heat transfer is dominated by diffusive transport. This effect was observed for the Ra of 10^4, being more present in the case of CP and less pronounced in the cases of CR$_{AIR}$ and CR$_{CO2}$. It was found that as the Ra increased, the warmer fluid layers expanded towards the top of the cold wall. This behavior was more pronounced in the CP case. It can also be observed that for Ra 10^5 and 10^6, for the CP case the isotherms tended to remain

horizontal in the center of the enclosure, presenting a high thermal stratification. For the CR$_{AIR}$ case, the effect of radiation reduced the temperature gradient across gravity. It is also noted that the temperature distribution was even more homogeneous for the CR$_{CO2}$ case. When radiation effects are present, near the active walls the temperature gradients increase, as a result of the temperature distribution in the medium, which leads to a temperature homogenization. This is more pronounced for higher Rayleigh numbers, due to the increased convection heat transfer mechanism. These results are in agreement with those found by Moufekkir *et al*. (2012b) working with conjugate heat transfer in an enclosure filled with an isotropic scattering medium.

The temperature distribution of the enclosure with protrusions for the cases evaluated in this study and the Ra ranging from 10^4 to 10^6 can be seen in Fig. 8. A thermal behavior similar to that observed for the enclosure without protrusions was verified. Thermal stratification in the center of the enclosure was observed for all Ra for the case of CP, whereas in cases where the thermal radiation was coupled, a more homogeneous temperature distribution is observed, this effect is more pronounced for the case of CR$_{CO2}$. It can also be observed that the presence of protrusions caused part of the fluid layer to be confined close to the walls. The thickness of the fluid layers located near the hot and cold walls, that is, with temperatures close to 50 °C and 40 °C, decreases as the number of Ra increases and in cases where the radiation is coupled. It is also noted that the presence of protrusions reduced the stratification zone for the case of CP and provided a better temperature distribution for the CR$_{AIR}$ and CR$_{CO2}$ cases.
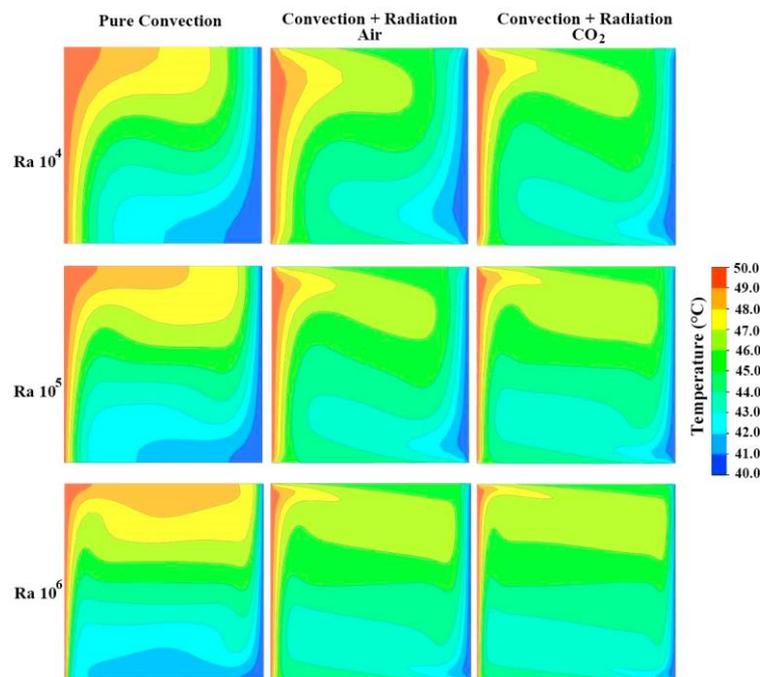
Fig. 7. Isotherms of the evaluated cases CP (left), CR$_{AIR}$ (middle), and CR$_{CO2}$ (right) as a function of the number of Ra for the enclosure without protrusions.
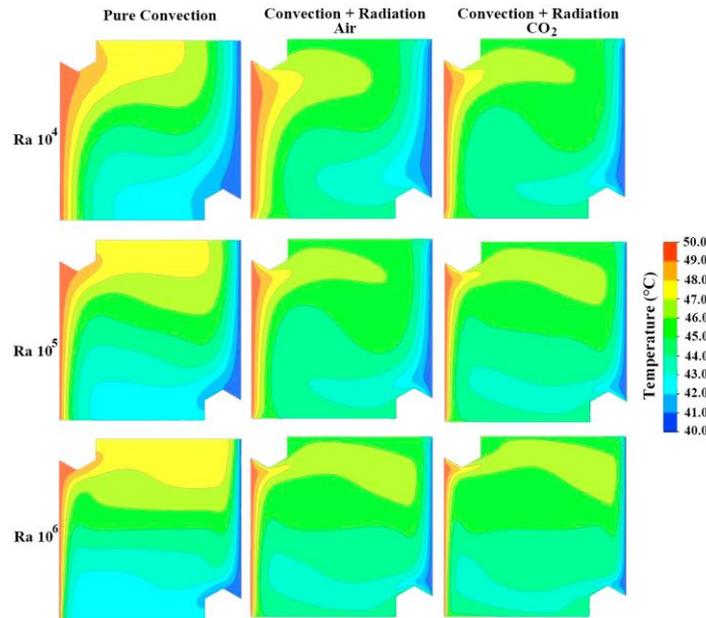
Fig. 8. Isotherms of the evaluated cases CP (left), CR$_{AIR}$ (middle), and CR$_{CO2}$ (right) as a function of the number of Ra for the enclosure with protrusions.
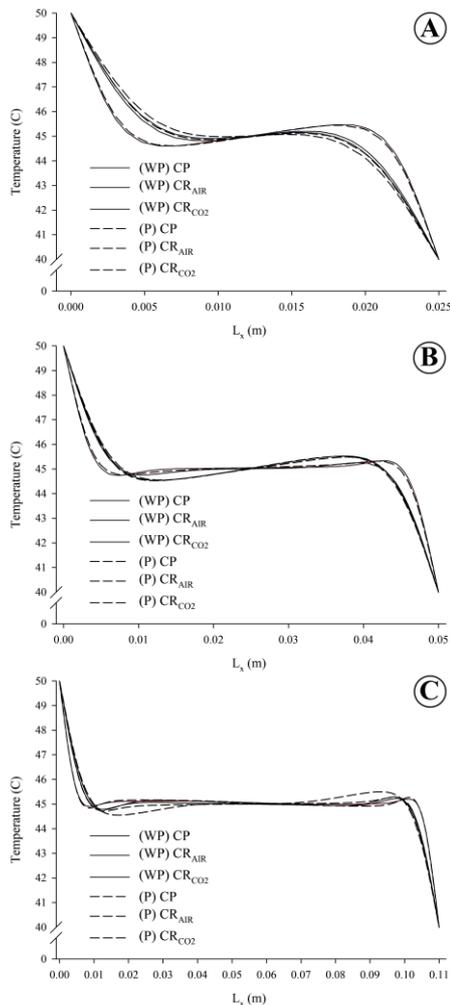
Fig. 9. Temperature profiles along the enclosure in the x-axis direction for (A) L = 0.025m (Ra = 10^4); (B) L = 0.050m (Ra = 10^5) and (C) L = 0.110 m (Ra = 10^6).

To verify the temperature profile between the two differentially heated walls, temperature data were also obtained on a horizontal line drawn in the center of the enclosure, and can be seen in Fig. 9. It is observed that the increase in the distance between the walls, and consequently in the Rayleigh number, makes the temperature profile more homogeneous in the center of the enclosures. This is because, as the Rayleigh number increases, thin boundary layers begin to form near the vertical walls, and the central region becomes progressively more stagnant. This behavior where the largest temperature gradients are located near the vertical walls was also observed experimentally by Ampofo and Karayiannis (2003) and numerically by Moufekkir *et al*. (2012a). For L = 0.025 m (Fig. 9a) there is a difference in temperatures referring to the cases of participant medium. This result is related to the interaction of the fluid (CO_2) with the heat exchange by radiation along with the enclosure. This difference is less pronounced and tends to decrease with increasing L.

4.3. Heat Transfer

Figure 10 shows the average variation of the Nusselt number (Nu$_m$) according to the increase of the Rayleigh number (Ra) for enclosures with and without protrusion. It can be observed that the radiation strongly influences the Nu$_m$. This is evident when it is verified that the scenario where only natural convection was considered (CP), presented the lowest values of Nu$_m$. There was also a direct relationship between Ra and Nu$_m$, which is, as the Ra increased, there was also an increase in Nu$_m$. These results are in agreement with the results obtained by Serrano-Arellano and Gijón-Rivera (2014) in their study on the conjugated heat transfer in a square enclosure.

For cases without protrusion, it is observed that Nu$_m$ ranged from 2.24 to 9.08 for CP, from 7.75 to 36.34 for CR$_{AIR,}$ and from 13.63 to 64.33 for CR$_{CO2}$. For
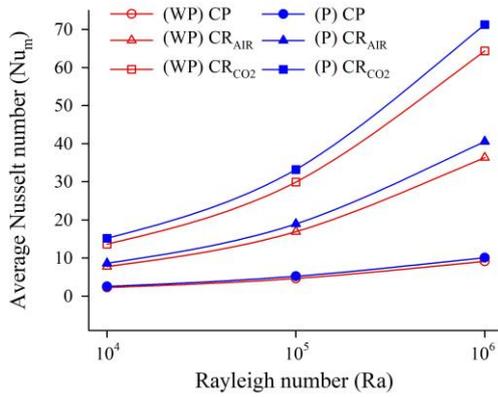
Fig. 10. Variation of the average Nusselt number in the enclosure without protrusion (WP) and with protrusion (P) as a function of the Rayleigh number for the cases of pure convection (CP) and combined convection and radiation with air (CR$_{Air}$) and CO$_2$ (CR$_{CO2}$) as the working fluid.

cases with a protrusion, Nu$_m$ ranged from 2.53 to 10.06 for CP, from 8.59 to 40.56 for CR$_{AIR}$, and from 15.16 to 71.23 for CR$_{CO2}$. For both geometries (with and without protrusion) the Nu$_m$ obtained for the case of CR$_{CO2}$ were on average about 7 times higher than those found for the case of CP for the assessed Ra range. It is observed that for all cases, the geometry without protrusion presented the lowest Nu$_m$ indicating that the insertion of the protrusion increases the heat transfer in the enclosure. The mean difference observed between cases with and without protrusion was approximately 11.5%.

The heat flux variation as a function of Ra and in the different enclosures is shown in Table 3. It is observed that regardless of the configuration or analysis performed, the values of heat flow reduce increase with the reduction of Ra. It appears that the CR$_{AIR}$ and CR$_{CO2}$ cases had the highest and intermediate values of heat flow, respectively. The heat flow values for the CR$_{AIR}$ case were more than three times higher than those presented for the CP case for any Ra value. This indicates that the effect of radiation on heat transfer in enclosures must be considered even in low temperature conditions, as evidenced by Rahimi and Sabernaeemi (2011) and Dehbi *et al.* (2019). The heat flow values varied between 23.71 and 101.10 W m^{-2} for scenarios without protrusion and 23.96 and 101.80 W m^{-2} for scenarios with protrusion.

5. CONCLUSION

A CFD analysis of different enclosure configurations for different Rayleigh numbers was performed in this study. The model proposed in this study was validated with the data available in the literature. The following results are concluded:

- The presence of protrusions in the evaluated enclosure causes a greater part of the current lines to present at higher speeds when compared to an enclosure without protrusions indicating more intense flows. The increase in the Rayleigh number directly influenced the maximum velocities observed for both enclosures, with increases greater than 100%.

- It was found that the presence of protrusions in the enclosure reduces the thermal stratification zone for the case of CP and provides a better temperature distribution for the CR$_{AIR}$ and CR$_{CO2}$ cases when compared to the cases without protrusions.

- The local acceleration of the streamlines close to the walls as a consequence of the increase in the Rayleigh number intensifies the heat exchange, generating greater temperature gradients close to the walls, while a more stagnant zone is verified in the center of the cavity.

- For all cases evaluated, an increase of about 75% in the Nusselt number was verified when using the participant medium, compared to the case with conjugated radiation and non-participating fluid, indicating an increase in heat transfer in the enclosure. The effect of coupling the radiation is more significant than the use of the participating medium except for the Nusselt number.

- Increasing the Rayleigh number provides an increase in the mean Nusselt number. Higher values of Nusselt numbers are also observed with the coupling of radiation in the energy equation. In both enclosures, the heat flow values for the CR$_{AIR}$ case are more than three times higher compared to pure convection cases for any value of the Rayleigh number. This indicates that the effect of radiation on heat transfer in enclosures must be considered even in low temperature conditions.

Table 3 Average heat flow (q'' - W m^{-2}) for the different Rayleigh numbers and types of enclosure evaluated.

Configuration	Rayleigh number	Pure convection	Conjugated (Air)	Conjugated (CO$_2$)
Without protrusion	10^4	29.18	101.10	97.98
	10^5	26.82	98.04	96.15
	10^6	23.71	94.84	93.10
With protrusion	10^4	29.99	101.80	97.95
	10^5	26.93	99.39	96.74
	10^6	23.96	95.79	93.79

REFERENCES

Abu-nada, E. and H. F. Oztop (2009). Effects of inclination angle on natural convection in enclosures filled with Cu–water nanofluid. *International Journal of Heat and Fluid Flow* 30 (4), 669-678.

Ahmed, S. E., H. F. Oztop and K. Al-Salem (2014). Natural convection coupled with radiation heat transfer in an inclined porous cavity with corner heater. *Computers & Fluids* 102 (Oct.), 74-84.

Ampofo, F. and T. G. Karayiannis (2003). Experimental benchmark data for turbulent natural convection in an air filled square cavity. *International Journal of Heat and Mass Transfer* 46 (19), 3551-3572.

Araujo, M. E. A., E. G. Barbosa, M. A. Martins and P. C. Corrêa (2022). Conjugated analysis of heat transfer by natural convection and radiation in a fin array using a semitransparent fluid medium. *Heat and Mass Transfer* 58 (Jan.), 1119–1132.

Baïri, A. (2008). Nusselt–Rayleigh correlations for design of industrial elements: Experimental and numerical investigation of natural convection in tilted square air filled enclosures. *Energy Conversion and Management* 49 (4), 771-782.

Bajorek, S. M. and J. R. Lloyd (1982). Experimental Investigation of Natural Convection in Partitioned Enclosures. *Journal of Heat Transfer* 104 (3), 527-532.

Bilgen, E. and H. Oztop (2005). Natural convection heat transfer in partially open inclined square cavities. *International Journal of Heat and Mass Transfer* 48 (8)**,** 1470-1479.

Cui, Y., Y. Wang, Q. Huang and S. Wei (2016). Effect of radiation and convection heat transfer on cooling performance of radiative panel. *Renewable Energy* 99 (Dec.), 10-17.

Dehbi, A., S. Kelm, J. Kalilainen and H. Mueller (2019). The influence of thermal radiation on the free convection inside enclosures. *Nuclear Engineering and Design* 341 (Jan.), 176-185.

Eby, S. D., J. Y. Trepanier and X. D. Zhang (1998). Modelling radiative transfer in SF6 circuit-breaker arcs with the P-1 approximation. *Journal of Physics* 31 (13), 1578–1588.

Gireesha, B. J., G. Sowmya, M. I. Khan and H. F. Öztop (2020). Flow of hybrid nanofluid across a permeable longitudinal moving fin along with thermal radiation and natural convection. *Computer Methods and Programs in Biomedicine* 185 (Mar.), 105166.

Goebel, F. and C. Mundt (2011, April). Implementation of the P1 radiation model in the CFD solver NSMB and investigation of radiative heat transfer in the SSME main combustion chamber. *17th AIAA International Space Planes and Hypersonic Systems and Technologies Conference*, San Francisco, USA.

Goodarzi, M., M. R. Safaei, H. F. Oztop, A. Karimipour, E. Sadeghinezhad, M. Dahari, S. N. Kazi and N. Jomhari (2014). Numerical Study of Entropy Generation due to Coupled Laminar and Turbulent Mixed Convection and Thermal Radiation in an Enclosure Filled with a Semitransparent Medium. *The Scientific World Journal* 2014 (Mar.), 761745, 1-8.

Ibrahim, A., D. Saury and D. Lemonnier (2013). Coupling of turbulent natural convection with radiation in an air-filled differentially-heated cavity at Ra = 1.5×10^9. *Computers & Fluids* 88 (Dec.), 115-125.

Karimipour, A. (2017). A novel case study for thermal radiation through a nanofluid as a semitransparent medium via discrete ordinates method to consider the absorption and scattering of nanoparticles along the radiation beams coupled with natural convection. *International Communications in Heat and Mass Transfer* 87 (Oct.), 256-269.

Li, X. and J. Tu (2019). Evaluation of the eddy viscosity turbulence models for the simulation of convection–radiation coupled heat transfer in indoor environment. *Energy and Buildings* 184 (Feb.), 8-18.

Meftah, S., A. Ibrahim, D. Lemonnier and A. Benbrik (2009). Coupled radiation and double diffusive convection in nongray Air-CO_2 and air-h_2o mixtures in cooperating situations. *Numerical Heat Transfer, Part A: Applications: An International Journal of Computation and Methodology* 56 (1), 1-19.

Meng, X., Y. Wang, T. Liu, X. Xing, Y. Cao and J. Zhao (2016). Influence of radiation on predictive accuracy in numerical simulations of the thermal environment in industrial buildings with buoyancy-driven natural ventilation. *Applied Thermal Engineering* 96 (Mar.), 473-480.

Mikhailenko, S. A., I. V. Miroshnichenko and M. A. Sheremet (2021). Thermal radiation and natural convection in a large-scale enclosure heated from below: Building application. *Building Simulation* 14 (Jul.), 681-691.

Miroshnichenko, I. V., M. A. Sheremet and A. A. Mohamad (2016). Numerical simulation of a conjugate turbulent natural convection combined with surface thermal radiation in an enclosure with a heat source. *International Journal of Thermal Sciences* 109 (Nov.), 172-181.

Modest, M. F. (2013). *Radiative heat transfer.* Academic Press: San Diego, California, USA, 2013, 896p.

Moufekkir, F., M. A. Moussaoui, A. Mezrhab, D. Lemonnier and H. Haji (2012a). MRT-lattice Boltzmann computations of natural convection and volumetric radiation in a tilted square enclosure. *International Journal of Thermal Sciences* 54 (Apr.), 125-141.

Moufekkir, F., M. A. Moussaoui, A. Mezrhab, H. Naji and D. Lemonnier (2012b). Numerical prediction of heat transfer by natural convection and radiation in an enclosure filled with an isotropic scattering medium. *Journal of Quantitative Spectroscopy and Radiative Transfer* 113 (13), 1689-1704.

Nia, M. F., S. A. G. Nassab and A. B. Ansari (2018). Transient combined natural convection and radiation in a double space cavity with conducting walls. *International Journal of Thermal Sciences* 128 (Jun.), 94-104.

Oguntala, G., G. Sobamowo and R. Abd-Alhameed (2019). Numerical analysis of transient response of convective-radiative cooling fin with convective tip under magnetic field for reliable thermal management of electronic systems. *Thermal Science and Engineering Progress* 9 (Mar.), 289-298.

Patil, S., A. K. Sharma and K. Velusamy (2016). Conjugate laminar natural convection and surface radiation in enclosures: Effects of protrusion shape and position. *International Communications in Heat and Mass Transfer* 76 (Aug.), 139-146.

Pishkar, I., B. Ghasemi, A. Raisi and S. M. Aminossadati (2022). Simulation of variable magnetic field effect on natural convection heat transfer of fe_3o_4/graphite slurry based on experimental properties of slurries. *Journal of Applied Fluid Mechanics* 15 (1), 1-14.

Rahimi, M. and A. Sabernaeemi (2011). Experimental study of radiation and free convection in an enclosure with under-floor heating system. *Energy Conversion and Management* 52 (7), 2752-2757.

Rashidi, I., O. Mahian, G. Lorenzini, C. Biserni and S. Wongwises (2014). Natural convection of Al2O3/water nanofluid in a square cavity: Effects of heterogeneous heating. *International Journal of Heat and Mass Transfer* 74 (Jul.), 391-402.

Saedodin, S. and M. S. M. Barforoush (2014). Comprehensive analytical study for convective–radiative continuously moving plates with multiple non-linearities. *Energy Conversion and Management* 81 (May), 160-168.

Saha, S. and Y. T. Gu (2015). Natural convection in a triangular enclosure heated from below and non-uniformly cooled from top. *International Journal of Heat and Mass Transfer* 80 (Jan.), 529-538.

Saravanan, S. and N. Raja (2020). Combined radiation-convection in an air filled enclosure with in-line heaters. *International Communications in Heat and Mass Transfer* 110 (Jan.), 104399.

Serrano-Arellano, J. and M. Gijón-Rivera (2014). Conjugate heat and mass transfer by natural convection in a square cavity filled with a mixture of Air–CO_2. *International Journal of Heat and Mass Transfer* 70 (Mar.), 103-113.

Sharma, A. K., K. Velusamy, C. Balaji and S. P. Venkateshan (2007). Conjugate turbulent natural convection with surface radiation in air filled rectangular enclosures. *International Journal of Heat and Mass Transfer* 50 (3-4), 625-639.

Siegel, R., J. R. Howell and M. P. Mengüç (2010). *Thermal Radiation Heat Transfer.* Boca Raton, FL, USA: CRC Press.

Tsuji, N., M. Nakano, E. Takada, K. Tokuhara, K. Ohashi, F. Okamoto, Y. Tazawa, Y. Inaba and Y. Tachibana (2014). Study of the applicability of CFD calculation for HTTR reactor. *Nuclear Engineering and Design* 271 (May), 564-568.

Valh Davis, G. (1983). Natural convection of air in a square cavity: a bench mark numerical solution. *International Journal for Numerical Methods in Fluids* 3 (3), 249-264.

Vivek, V., A. K. Sharma and C. Balaji (2012). Interaction effects between laminar natural convection and surface radiation in tilted square and shallow enclosures. *International Journal of Thermal Sciences* 60 (Oct.), 70-84.

Wang, Y., X. Meng, X. Yang and J. Liu (2014). Influence of convection and radiation on the thermal environment in an industrial building with buoyancy-driven natural ventilation. *Energy and Buildings* 75 (Jun.), 394-401.